# Helios-1 Faraday Rotation Experiment:
# Results and Interpretations
# of the Solar Occultations in 1975

H. Volland and M.K. Bird

Radioastronomisches Institut, Universität Bonn,
Auf dem Hügel 71, D-5300 Bonn, Federal Republic of Germany

G.S. Levy, C.T. Stelzried, and B.L. Seidel

Jet Propulsion Lab., Pasadena CA 91103, U.S.A.

**Abstract.** The polarization angle of the HELIOS-1 downlink signal has been monitored during two solar occultations in 1975 at two widely separated ground stations. Significant Faraday rotation of the signal occurs whenever the signal ray path passes through the solar corona near superior conjunction. Large-scale variations in the data arise both from rotation of the solar corona and from the slowly changing solar offset (point of smallest heliocentric distance along ray path). A simplified model of the solar corona has been developed to simulate the results of the Faraday rotation measurements. In this model the known polarity of the large-scale interplanetary magnetic field is employed as an aid in determination of the product $N \cdot B$ (electron density × magnetic field) as a function of heliographic longitude and heliocentric distance $r$ within $2$–$10 R_{\odot}$. In this distance range $N \cdot B$ is proportional to $r^{-5.5}$. If the magnetic field can be assumed to follow an inverse square law over this range, the electron density is found to be decreasing as $r^{-3.5}$, in good agreement with previous results. The derived longitudinal structure for the corona during both occultations is consistent with synoptic coronal white light observations.

**Key words:** Faraday rotation — Corona — Solar Occultation.

## 1. Introduction

Two solar occultations of the satellite HELIOS-1 occurred in 1975. The first one was in the latter half of April when the satellite's ray path approached the west limb of the Sun to a minimum distance of 1.63 solar radii (Fig. 1) and the second one took place in late August/early September when HELIOS-1 was totally eclipsed by the photosphere (Fig. 2). Measurements of the polarization angle of the linearly polarized telemetry signal were performed with automatic tracking polarimeters at the 64 m Goldstone Tracking Station of the NASA Deep Space Network in California, and also at the 100 m radio telescope of the Max-Planck-
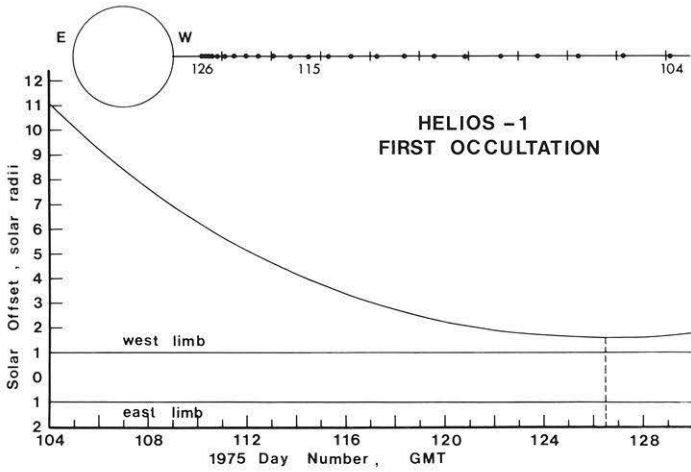
**Fig. 1.** Solar offset (ray path parameter) in solar radii during the first occultation of HELIOS-1 in 1975. The dashed vertical line denotes the epoch of minimum approach of the HELIOS-Earth line-of-sight to the Sun
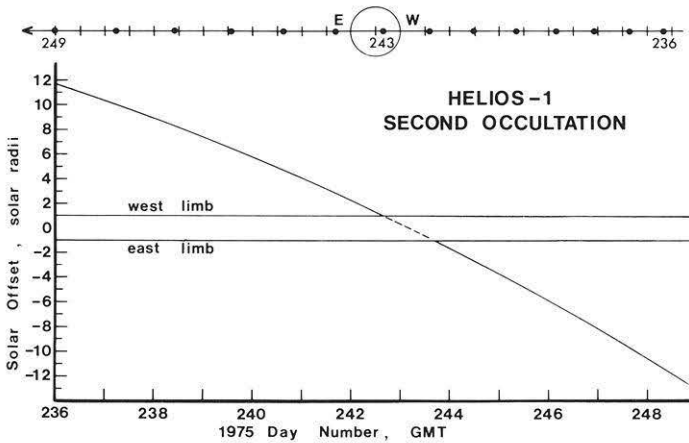


**Fig. 2.** Solar offset (ray path parameter) in solar radii during the second occultation of HELIOS-1 in 1975

Institut für Radioastronomie in Effelsberg near Bonn, Germany. The HELIOS-1 antenna transmits a linearly polarized carrier signal in the S-band (2.3 GHz), the electric vector being orthogonal to the ecliptic plane. The transformation of the orientation of the plane of polarization received on Earth to values referred to the ecliptic plane is straightforward (Stelzried et al., 1972).

## 2. Observations

Figures 3 and 4 show the polarization angle $\Omega$ (signal Faraday rotation) as a function of time (UT). The solar offset (minimum approach of signal ray path to
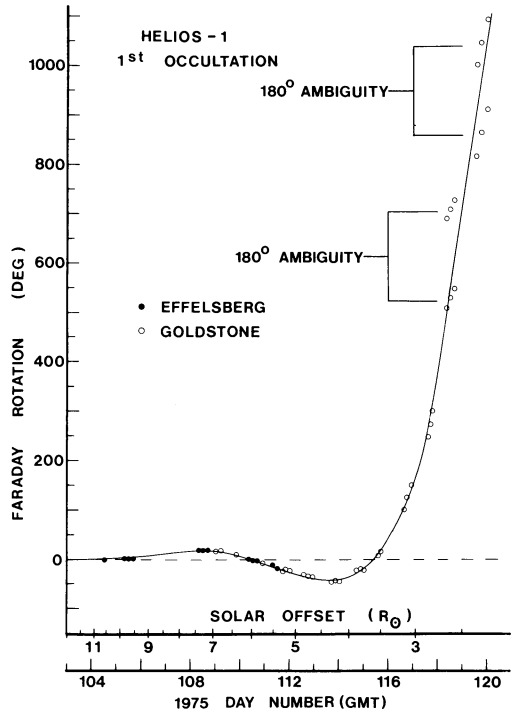
**Fig. 3.** Coronal Faraday rotation (uncorrected for ionosphere) versus solar offset during first occultation (circles: measurement; solid curve: theory). Note ambiguity on days 118–119
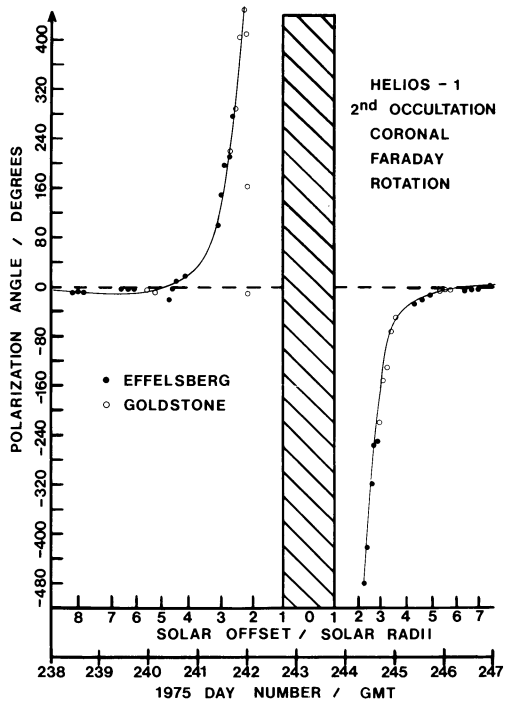


**Fig. 4.** Coronal Faraday rotation (uncorrected for ionosphere) versus solar offset during second occultation (circles: measurement; solid curve: theory)
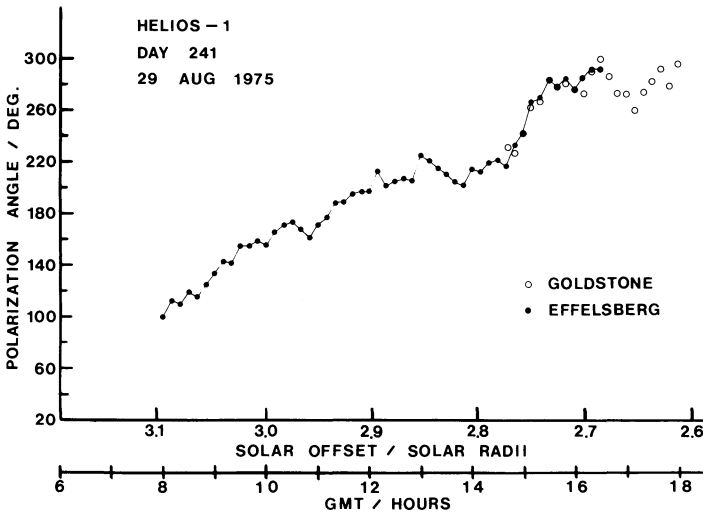
**Fig. 5.** Polarization angle (coronal Faraday rotation) measured on 1975 day no. 241 during the second occultation. Note overlapping of Goldstone and Effelsberg measurements

Sun) is also plotted along the abscissa. For both occultations the Goldstone measurements are denoted by open circles and Effelsberg by solid circles. The Faraday rotation of the signal is defined to be positive when the plane of polarization rotates counterclockwise as viewed from the receiver looking up at HELIOS. The maximum diurnal influence of the ionosphere is typically of the order of 4° at Goldstone and 2° at Effelsberg and is therefore neglected in this first order approximation. The ionospheric contribution to the observed Faraday rotation can be estimated from radio beacon experiment data from the geostationary satellites ATS-1 (at Goldstone) and ATS-6 (at Effelsberg). This correction will be incorporated into all subsequent analyses of HELIOS Faraday rotation data, but is not expected to· significantly effect the results of this paper. Similarly, no correction has been attempted here for the deviation of the spacecraft spin (antenna) axis from the normal to the ecliptic. The nominal configuration is specified at less than 0.5°.

Figure 5 shows a detailed registration plot taken on 1975 day no. 241, demonstrating that the fine structure of the variation of $\Omega$ is observed at Goldstone as well as at Effelsberg during times of overlapping station coverage, and therefore is caused very probably by coronal effects. The design of the automatic tracking polarimeters (see Ohlson et al., 1974) theoretically allows for a measurement of $\Omega$ to an accuracy less than 0.5° for effective system time constants $\tau \simeq 30\text{--}100\,\text{s}$. Increase in system operating noise due to solar radiation in the antenna sidelobes can raise the error to typically 5° at solar offsets around $3\,R_\odot$. The polarimeters are incapable of recording variations in $\Omega$ with characteristic periods smaller than $\tau$. Moreover, Figure 5 clearly demonstrates the importance of employing at least two widely separated stations in order to resolve the 180° ambiguity at one station alone due to the missing nighttime data. A surprising result during both occultations was that one was able to

follow the telemetry signal to offsets as near to the Sun as 2 solar radii and to observe variations in $\Omega$ up to 800°. This is in contrast to earlier experiments (Stelzried et al., 1970) where only values $\Delta\Omega < 130°$ at distances no nearer than 4 solar radii have been registered. There are two primary reasons for this: (a) HELIOS-1 had a better signal-to-noise ratio than the previous measurements due to higher antenna gain and transmitter power, and (b) the earlier occultations occurred in 1968 near solar maximum, while the HELIOS-1 occultations in 1975 took place during a solar cycle minimum. The closer approach of the HELIOS-1 ray path to the Sun and the two station coverage during the occultation phases of the mission render the present data much more amenable to a quantitative interpretation. In particular, because of the solar minimum conditions, we expect rather regular and long-lasting features on the Sun which may assist in the formulation of an unambiguous interpretation of the results.

## 3. Theory

The magnetic field and electron density structure within the outer corona (2–10 solar radii) may be rather complicated. Direct measurements in this region are limited mainly to disturbed (flare and burst) conditions (Hildner et al., 1975). The values of the electron density during quiet conditions are based primarily on photometric measurements of the integral white coronal light during solar eclipses (Newkirk, 1967). An experimentally determined form for the magnetic field in this region during quiet conditions virtually does not exist to our knowledge. The magnetic field can be inferred from the magnetic configuration observed on the photosphere (see, for example, Schatten et al., 1969, and Newkirk et al., 1972). On the other hand, it is well known that at least beyond 0.3 AU the solar wind shows a simple sector structure which can be very stable over many solar rotations (Svalgaard and Wilcox, 1975). A two-sector structure has prevailed in interplanetary space since about 1972 which can be observed either on or near the Earth (Hedgecock, 1975; Svalgaard et al., 1974) as well as on board HELIOS (Neubauer and Musmann, 1976). In each sector the interplanetary magnetic field is unipolar and changes its polarity from one sector to the next. The electron density as well as the radial component of the interplanetary magnetic field (IMF) decrease within each sector proportionally to $r^{-2}$. The general solar magnetic field as deduced if the Sun is seen as a star seems to be related to the structure and polarity of the IMF (Severny et al., 1970). Moreover enhanced intensities in the coronal white light (Hansen et al., 1974) seem to be related to the sector boundaries. The closed magnetic field lines within the streamers seldom reach beyond 2 solar radii (Newkirk et al., 1972).

Because of this limited knowledge about the outer corona we have attempted to try first a model which is as simple as possible, yet accounts for a basic sector structure in heliographic longitude. Although variations in heliographic latitude are certainly present (Rosenberg and Coleman, 1969; Rosenberg, 1975) over the ±7° covered by the HELIOS ray path, they are considered to be considerably weaker than the longitudinal variation and are therefore neglected. We further assume a single power law radial dependence of the electron density $N$ and radial
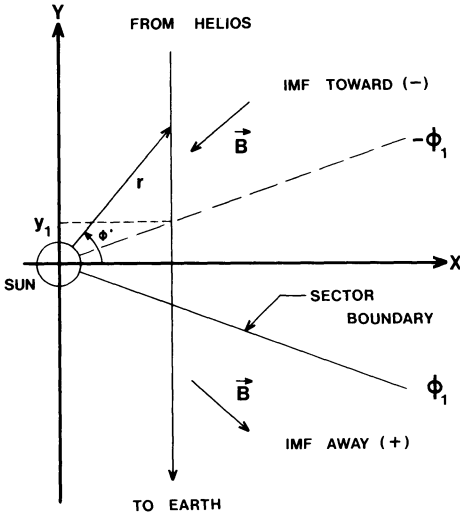
**Fig. 6.** Geometric configuration of system HELIOS-Sun-Earth for a single regional boundary on the west limb at $\phi = \phi_1$. The region from $-y_1$ to $+y_1$ makes no contribution to the net Faraday rotation of the signal

component of the magnetic field $B_r$ in each sector, and neglect other components of **B** in our region of interest $(2R_\odot < r < 10R_\odot)$:

$$N = N_i r^{-\alpha}; \qquad B_r = B_i r^{-\beta} \tag{1}$$

with $N_i$, $B_i$ values extrapolated to the solar surface in the $i^{th}$ sector and $r$ the distance from the Sun in solar radii. $\alpha$ and $\beta$ are exponents to be determined and are assumed to be the same in all sectors. $B_i$ negative (positive) is associated with toward (away) sector polarity.

At S-band $(\lambda = 13\ cm)$ one may employ a simplified expression for the electron induced Faraday rotation along a given ray path (e.g. Stelzried et al., 1970). This "quasi-longitudinal approximation" is valid for the case when (a) the frequency $f$ meets the criteria $f \gg f_c$, $f \gg f_g$, $f \gg f_p$, where $f_c$, $f_g$ and $f_p$ are the electron collision, electron Larmor, and plasma frequencies respectively, and (b) the wave does not travel transverse to the magnetic field. Under these conditions, which are easily satisfied by the HELIOS signal propagating through the solar corona and ionosphere, the Faraday rotation is given by

$$\Omega = \frac{K}{f^2} \int_s N\,\mathbf{B} \cdot \mathbf{ds} \qquad \text{radians} \tag{2}$$

where

$K = 2.36 \times 10^4$      in mks units.

$f = 2.296\ \text{GHz}$

Since refraction in our region of interest in the solar corona is negligible, the straight line ray path geometry shown in Figure 6 can be employed to reduce (2)

to the more practical form

$$\Omega = C \int_{-\infty}^{\infty} N B_r \sin\phi \, dy \quad \text{degrees} \tag{3}$$

with

$C = 1.786 \times 10^{-4} \quad$ in mks units if

$N$ is in electrons/m$^3$

$B_r$ is in Tesla

$dy$ is in solar radii.

Assuming one sector boundary on the west limb at the angle $\phi_1$ with the Earth in sector number 1 (Fig. 6), one obtains from symmetry arguments and by combining (1) with (3):

$$\Omega = C(N_1 B_1 - N_2 B_2) \int_{Y_1}^{\infty} \frac{y \, dy}{r^{\alpha+\beta+1}} = \frac{C D_1}{\gamma} \left(\frac{\cos\phi_1}{x}\right)^{\gamma} \tag{4}$$

with

$x$ the solar offset of the ray path

$\gamma = \alpha + \beta - 1; \quad D_1 = (N_1 B_1 - N_2 B_2)$

$\phi_1 = \Phi_1 + \omega(t - t_0); \quad -90° \leq \phi_1 \leq 90° \tag{5}$

$\omega = 2\pi/27 \, \text{days} = 13.3 \, \text{deg/day}$

     = the angular frequency of the solar rotation

$\Phi_1 =$ the angle of the sector boundary from the $x$-axis at the time $t_0$.

Calculations for the east limb ($x < 0$, $90° < \phi_1 < 270°$) require that $D_1 \rightarrow -D_1$ in the above.

    If we assume $m$ sectors with boundaries at the angular positions $\phi_{i-1}$, $\phi_i$, $\phi_{i+1}$, etc., we obtain the series

$$\Omega = \frac{C}{\gamma} (-1)^{\delta} \sum_{i=1}^{m} D_i \left(\frac{\cos\phi_i}{x}\right)^{\gamma} \tag{6}$$

with

$-90° \leq \phi_i \leq 90°; \quad \delta = 0 \quad \text{west limb,}$

$90° \leq \phi_i \leq 270°; \quad \delta = 1 \quad \text{east limb,}$

and

$D_i = N_i B_i - N_{i+1} B_{i+1}.$

The sectors are numbered sequentially starting at sector 1 and proceeding around the sun in a counterclockwise direction as viewed from above the ecliptic.

The sum (6) over "sector boundaries" to compute the theoretical Faraday rotation includes only those terms for which the quantity $(\cos\phi_i/x)$ is positive, otherwise the term is set equal to zero. This insures that the sum is extended only over those "boundaries" on the appropriate solar limb. It should also be noted that the sign of $N_i B_i$ in "sector" $i$ is not required to flip polarity across its boundaries. Therefore, Equation (6) may be viewed as a sum over regional subdivisions in heliographic longitude, each region characterized by its constant $N_i B_i$ and its width given by its boundaries $\phi_i$ and $\phi_{i-1}$. Many such regions may in fact be contained within a classical large-scale solar sector of uniform polarity.

## 4. Comparison between Observations and Theory

The time derivative of the Faraday rotation (6) is given by

$$\dot{\Omega} = -\gamma\Omega\,\frac{\dot{x}}{x} - C\omega(-1)^\delta \sum_{i=1}^{m} D_i \left(\frac{\cos\phi_i}{x}\right)^\gamma \tan\phi_i. \tag{7}$$

The first term of (7) arises from the motion of the spacecraft's solar offset in the corona, while the second term results from the rotation of the corona itself. At times of small solar offset and large spacecraft motion, achieved for example during the second occultation, one expects the first term of (7) to be dominant. Under these conditions one may estimate $\gamma$ from the slope of a plot $\ln\Omega$ vs. $\ln x$. Such estimates yield $\gamma \simeq 4.1$ at $x = \pm 3 R_\odot$. Due to the uncertainty in the second term of (7), however, one must accept a rather large tolerance on the allowed values of $\gamma$, especially if this parameter is to be approximated as a constant in the range $2$–$10 R_\odot$. In practice, values of $\gamma$ as low as 3.5 and as high as 5.0 were found to yield good fits to the Faraday data.

The terms of the sum (6) may be regrouped into a form more adaptable to model calculations by summing essentially over "regions" rather than "regional boundaries":

$$\Omega = \frac{C}{\gamma}(-1)^\delta \sum_{i=1}^{m} N_i B_i \{(\cos\phi_i/x)^\gamma - (\cos\phi_{i-1}/x)^\gamma\}. \tag{8}$$

There are then $2m+1$ parameters to be derived from a fit of (8) to the Faraday rotation observations: $\gamma$ and the $m$ pairs of regional weight factors $N_i B_i$ and boundaries $\Phi_i$. A systematic determination of the optimum model parameters was accomplished using the following program: (1) $\gamma$ was varied in steps of 0.5 over the range $3.0 < \gamma < 6.0$. (2) Two of the regional boundaries denoted by the $\Phi_i$ were fixed to conform with the location of sector boundaries inferred from polar cap observations during the occultation. This establishes two "large-scale" sectors for each model, within which one particular magnetic field polarity is dominant. (3) The remaining "free" regional boundaries are then varied over all
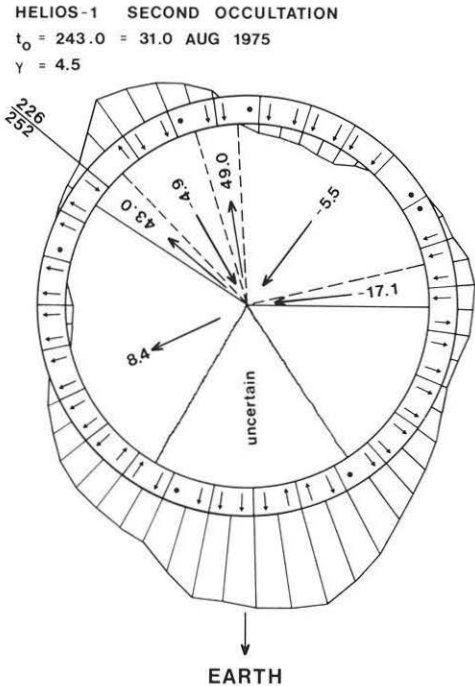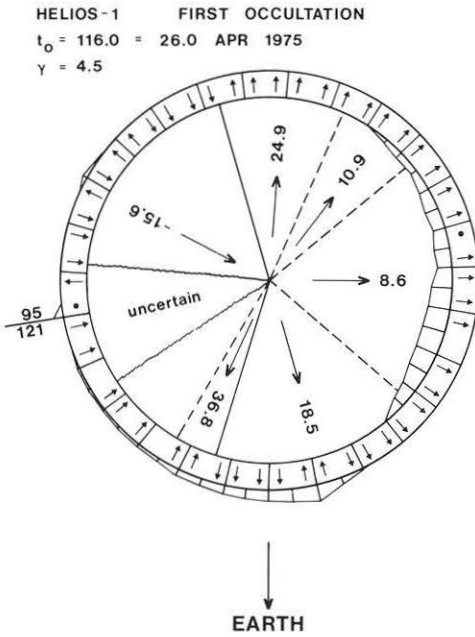
possible angular positions (except those occupied by the above mentioned two "fixed" boundaries) in steps of one day of solar rotation. A step size smaller than this is impractical, since localization of solar features in heliographic longitude from coronal white light or IMF measurements cannot be accomplished to an accuracy of better than one day anyway. The number of possible boundary configurations generated in this way is given by the binomial coefficient $\binom{j}{k}$, where $j$ = number of possible positions for a regional boundary = 25; $k$ = number of "free" regional boundaries. This results in 12,650 trial models for $m = 6$. (4) For a given set of regional boundaries and a given $\gamma$, the coronal structure is assumed to remain constant (rigid rotation) on a time scale at least comparable with the duration of the occultation. Each measurement of $\Omega$ thus yields a linear equation from (8) in the unknowns $N_i B_i$, $i = 1, m$. Selecting $n$ spaced measurements ($n > m$), the system is then solved for the set $N_i B_i$, $i = 1, m$ for which deviations between measured and computed values of $\Omega$ are minimized in the least-squares sense.

It should be noted that no demands are placed on the polarity of the various regions as controlled by the sign of the factor $N_i B_i$ when solving the normal equations for the best least-squares solution. Indeed, many models can be immediately rejected if the polarities of the regions disagree with those extrapolated from inferred polarities of the IMF made at Earth (Solar Geophys. Data, Nov. 1975). Similarly, some models yield magnitudes for the product $N_i B_i$ which are inconsistent with reasonable coronal values. Coronal models were rejected which contained $N_i B_i$ outside the range $10^7 < N_i B_i < 10^{10}$ Tesla $m^{-3}$.

It should be mentioned that polarity agreement within the large-scale sectors was considered to hold even if an occasionally isolated region within the sector was determined to have the wrong polarity as long as the width of that region was not greater than one day. This allows for the often observed smaller structures of opposite polarity that are apparent in interplanetary space. Requiring that each region conform in polarity to that in its respective large-scale sector results in a rejection of all trial models. It is thus apparent that some medium-scale structure is important for the generation of the observed Faraday rotation profile.

Although one goal of this analysis was to simulate the observed Faraday rotation time profile with the simplest possible coronal model, no satisfactory fit to the data could be accomplished with $m < 6$ using models with an acceptable set of $\gamma$ and $N_i B_i$, $i = 1, m$ under the above polarity and magnitude restrictions. Considerably better results are obtained for $m = 6$, at which point the coronal models have enough longitudinal structure to adequately follow the zeros and extrema observed in the Faraday data, and yet one is able to make a unique determination of the one basic coronal configuration which satisfies both the Faraday data and the restrictions on the polarity/magnitude of the $N_i B_i$. Models with $m > 6$ were not tested since the integral nature of the Faraday data does not justify attempts to determine a finer spatial resolution of solar features.

The absolutely best models for both occultations, based on minimum root-mean-square deviation of theoretical Faraday rotation from the observed one, were obtained for $m = 6$, $\gamma = 4.5$. For the first occultation only a small fraction

HELIOS-1    FIRST OCCULTATION
$t_0$ = 116.0 = 26.0 APR 1975
γ = 4.5

EARTH



HELIOS-1    SECOND OCCULTATION
$t_0$ = 243.0 = 31.0 AUG 1975
γ = 4.5

EARTH

**Fig. 7.** Inferred coronal structure as seen from above the ecliptic plane during the first occultation. The epoch (UT) is $t_0$ =116.0 days (26.0 APR 1975), and the power law exponent for the radial fall off of $N \cdot B$ is 5.5 ($\gamma$=4.5). Two of the six regional boundaries are fixed from IMF sector observations (solid radial lines), and the remaining four are free parameters determined from a least-squares analysis (dashed lines). The polarity and magnitude of the factors $N_i B_i$ are indicated in each region (unit: $10^8 \, T \, m^{-3}$). The outer circle displays the inferred IMF polarity, shifted 4.5 days, for the solar rotation from 1975 days 95–121. A black dot signifies "mixed polarity" or "effect doubtful or not discernable". No information about the region marked "uncertain" can be derived from the Faraday data, since the ray path did not probe these longitudes. Finally, the striped regions bounded by the radial plotted curves show the relative intensities of the west limb pB measurements at $1.5 R_\odot$ from R.T. Hansen et al., from which one infers a qualitative enhancement in electron density (curve outside outer circle) or a region of low density (curve inside inner circle)

**Fig. 8.** Inferred coronal structure during the second occultation (see Fig. 7 for explanation). The epoch (UT) is $t_0$ =243.0 days (31.0 AUG 1975), and $\gamma$=4.5. The interplanetary polarities are given for the solar rotation from 1975 days 226–252

(2.89 %) of the 12,650 trial models were found to yield acceptable values of $N_i B_i$. The eight acceptable models with the best fits to the Faraday data all display strong qualitative similarities (i.e. one regional boundary moved one day with correspondingly small adjustment in the associated value of $N_i B_i$), so that only one unique general configuration could be acclaimed compatible with all measurements. The theoretical Faraday rotation from the best fitting model not qualitatively similar to those first eight exhibited a much higher deviation from the observed and can be excluded from consideration.

The acceptable models with the best fits to the Faraday data are shown in Figures 7 and 8 for the first and second occultations respectively. The diagrams are "snapshots" of the rigidly rotating corona from above the north solar pole at the UT times $t_0 = 116.0$ days (first occultation) and $t_0 = 243.0$ days (second occultation). The theoretical Faraday rotation computed from (8) for these models is drawn as a solid curve in Figures 3 and 4. The polarity and value of the weight factor $N_i B_i$ (in units of $10^8$ Tesla $m^{-3}$) are indicated within each region. For comparison, the IMF direction inferred from polar cap magneto-grams are shown in the outer circle (Solar Geophys. Data, Nov., 1975). The inferred polarities are given for the time period between the days on either side of the solar rotation "cut line" (extended radial line) and are shifted 4.5 days in time to account for the solar wind transit time to Earth. The region marked "uncertain" contains those heliographic longitudes not effectively probed by the HELIOS-Earth ray path during the occultation. Note that the second occultation (Fig. 8) occurred 4.7 solar rotations after the first one. Although coronal features are often observed to remain stable over such extended intervals, it is not really surprising that the detailed structure has undergone considerable redistribution. An indication that this is indeed the case for the interval between occultations is evident in the K-corona limb intensity measurements provided to us by R.T. Hansen and colleagues (private communication). The coronal pB (polarization × brightness) intensities at $1.5 R_\odot$ on the west limb can be interpreted as a qualitative measure of electron density. These measurements over one solar rotation yield the curves drawn in Figures 7 and 8 outside the outer circle (heliolongitudes with intensity above specified threshold) and inside the inner circle (below average intensity, or "coronal holes"). Qualitative agreement with the configurations derived from the Faraday data is evident for both occultations.

Figure 9 shows the electron density radial-profile obtained from the mean weighted values of $N_i B_i$ from the models in Figures 8 and 9, and also from models (not shown) with $\gamma = 4.0$. The magnetic field is assumed to be purely radial ($\simeq r^{-2}$) with a mean strength at the coronal base of 1 gauss. Also shown are a modified Allen-Baumbach profile with an extra term in $r^{-2}$ (Stelzried et al., 1970), and a model based on time-delay measurements during the occultations of Mariner-6 and Mariner-7 (Muhleman et al., 1977). The mean value of $N_i B_i$ increases with increasing $\gamma$, so that even the single-power approximation appears to be adequate over the range $2 R_\odot < r < 10 R_\odot$ for both models shown.

The data gaps on the last two days of the first occultation (Fig. 3) resulted in an unresolved $n\pi$ ambiguity in measured polarization angle. The best estimates of the probable values on these days were used in additional investigations to determine the influence of this effect on the derivation of a coronal model. Since
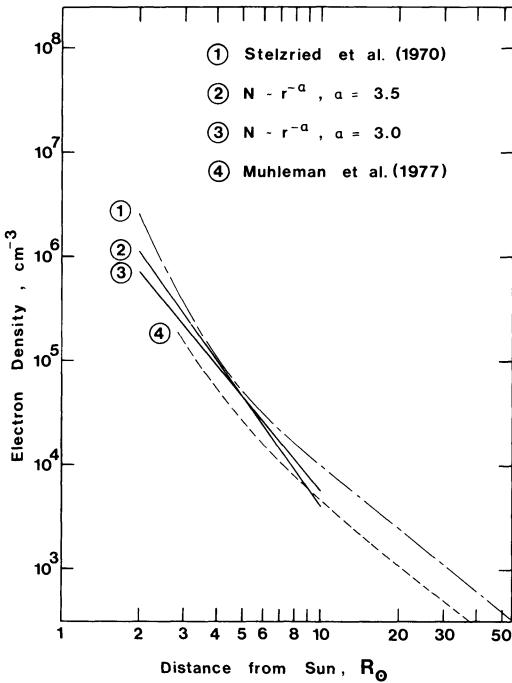
**Fig. 9.** Radial profile of the coronal electron density. The single power fall-off approximation to be used over the range $r = 2$–$10 R_\odot$ is a straight line in this representation. The mean value of $N_i B_i$ weighted over all regions has been computed for the models of Figures 7 and 8 ($\gamma = 4.5$) and also for two unpictured models ($\gamma = 4.0$). The electron density profile results if one assumes the magnetic field to be purely radial ($\simeq r^{-2}$) and has a strength of 1 gauss at the solar surface. This yields electron density fall off rates $\alpha = 3.0$ and 3.5 (Curves 3 and 2). The approximations are reasonably close to the semi-empirical models (Curves 1 and 4), at least over the radial range of interest for Faraday rotation data

a considerably poorer fit to the observations was realized upon fitting to the upper points of Figure 3, one is inclined to prefer the lower values.

The sharp drop in measured Faraday rotation toward the end of day 241 during the second occultation (Fig. 4) cannot be due to the slowly varying solar offset and rotation solar corona. The abrupt decline is similar to the initial phase of the "transient events" seen during the occultation of Pioneer 6 near solar maximum (Levy et al., 1969). Measurements during the event were ignored for the quiet corona simulation attempted in this work.

## 5. Summary and Conclusions

A simplified model of the solar corona has been developed to simulate the results of Faraday rotation measurements taken during the two 1975 solar occultations of the satellite HELIOS-1. The sun is divided into $m$ "regions" of arbitrary width in heliographic longitude, within which the electron density $N$ and the radial magnetic field $B_r$ are assumed to decrease with radial distance according to a simple power law. The values of the product $N \cdot B_r$ at the solar surface, $N_i B_i$, $i = 1, m$ within each region are determined from a least-squares solution to a set of normal equations of the form (8) for all possible locations of the "regional boundaries". Two of these boundaries are fixed from the observed positions of the large-scale sector boundaries in interplanetary space.

The radial dependence of the product $N_i B_i$ from $2-10 R_\odot$ is found to fall off as $r^{-5.5}$. The longitudinal structure is sufficiently complex that the data cannot be adequately simulated for $m < 6$. With 6 regions one obtains only a small fraction of the original trial models for which the values of $N_i B_i$ are both compatible with the direction of the inferred interplanetary magnetic field and also lie within the range of observed coronal magnitudes. The quality of the fits of these compatible coronal models to the Faraday data ranges from very poor to excellent. In the two cases investigated, a smaller subgroup of coronal configurations with very similar parameter values provided a least-squares fit far superior to all remaining contending models. The hypothesis that this subset of trial models defines a basically "unique" coronal configuration is supported by their qualitative agreement with synoptic white light coronal observations.

Future studies will include a comparison of such derived models with solar radio observations and with electron densities inferred from the HELIOS ranging experiment (Edenhofer et al., 1977). The method introduced here will be refined and expanded upon in an effort to improve the convergence to a unique coronal configuration, while retaining an inherently simple model basis.

## References

Edenhofer, P., Esposito, P.B., Hansen, R.T., Hansen, S.F., Lüneburg, E., Martin, W.L., Zygielbaum, A.I.: Time delay occultation data of the Helios spacecrafts and preliminary analysis for probing the solar corona. J. Geophys. 42, 673–698, 1977

Hansen, S.F., Sawyer, C., Hansen, R.T.: K corona and magnetic sector boundaries. Geophys. Res. Lett. 1, 13–15, 1974

Hedgecock, P.C.: The heliographic latitude dependence and sector structure of the interplanetary magnetic field 1969–1974: Results from the HEOS satellites. Solar Phys. 44, 205–224, 1975

Hildner, E., Gosling, J.T., MacQueen, R.M., Munro, R.H., Poland, A.I., Ross, C.L.: The large coronal transient of 10 June 1973, I: Observational description. Solar Phys. 42, 163–177, 1975

Levy, G.S., Sato, T., Seidel, B.L., Stelzried, C.T., Ohlson, J.E., Rusch, W.V.T.: *Pioneer 6:* Measurement of transient Faraday rotation phenomena observed during solar occultation. Science 166, 596–598, 1969

Muhleman, D.O., Esposito, P.B., Anderson, J.D.: The electron density profile of the outer corona and the interplanetary medium from *Mariner-6* and *Mariner-7* time-delay measurements. Astrophys. J. 211, 943–957, 1977

Neubauer, F.M., Musmann, G.: Observation of magnetic sector structure and streams during the primary mission of HELIOS-1. Paper presented at Helios Project Seminar on Scientific Results, Bonn, 19–21 May 1976

Newkirk, Jr., G.: Structure of the solar corona. Ann. Rev. Astron. Astrophys. 5, 213–266, 1967

Newkirk, Jr., G., Trotter, D.E., Altschuler, M.D., Howard, R.: Atlas of magnetic fields in the solar corona. Solar Phys. 24, 370–372, 1972

Ohlson, J.E., Levy, G.S., Stelzried, C.T.: A tracking polarimeter for measuring solar and ionospheric Faraday rotation of signals from deep space probes. Trans. IEEE 23, 167–177, 1974

Rosenberg, R.L.: Heliographic latitude dependence of the IMF dominant polarity in 1972–1973 using Pioneer 10 data. J. Geophys. Res. 80, 1339–1340, 1975

Rosenberg, R.L., Coleman, Jr., P.J.: Heliographic latitude dependence of the dominant polarity of the interplanetary magnetic field. J. Geophys. Res. 74, 5611–5622, 1969

Schatten, K.H., Wilcox, J.M., Ness, N.F.: A model of interplanetary and coronal magnetic fields. Solar Phys. 6, 442–455, 1969

Severny, A., Wilcox, J.M., Scherrer, P.M., Colburn, D.S.: Comparison of the mean photospheric magnetic field and the interplanetary magnetic field. Solar Phys. 15, 3–14, 1970

Solar Geophysical Data, **375**, Nov. 1975

Stelzried, C.T., Levy, G.S., Sato, T., Rusch, W.V.T., Ohlson, J.E., Schatten, K.H., Wilcox, J.M.: The quasi-stationary coronal magnetic field and electron density as determined from a Faraday rotation experiment. Solar Phys. **14**, 440–456, 1970

Stelzried, C.T., Sato, T., Abreu, A.: Transformation of received signal polarization angle to the plane of the ecliptic. J. Spacecraft **9**, 69–70, 1972

Svalgaard, L., Wilcox, J.M.: Long term evolution of solar sector structure. Solar Phys. **41**, 461–475, 1975

Svalgaard, L., Wilcox, J.M., Duvall, T.L.: A model combining the polar and the sector structured solar magnetic fields. Solar Phys. **37**, 157–172, 1974